PAPER

Double-layered blood vessels over 3 mm in diameter extruded by the inverse-gravity technique

Biofabrication

PAPER

Double-layered blood vessels over 3 mm in diameter extruded by the inverse-gravity technique

Van Thuy Duong[1], Chanh Trung Nguyen[1], Huu Lam Phan[1], Van Phu Le[1], Thao Thi Dang[2], Cholong Choi[4], Jongmo Seo[3], Chaenyung Cha[4], Sung Hoon Back[2] and Kyo-in Koo[1,*]

[1] Department of Electrical, Electronic and Computer Engineering, University of Ulsan, Ulsan 44610, Republic of Korea
[2] School of Biological Sciences, University of Ulsan, Ulsan 44610, Republic of Korea
[3] Electrical and Computer Engineering, Seoul National University, Seoul 08826, Republic of Korea
[4] Center for Multidimensional Programmable Matter, Department of Materials Science and Engineering, Ulsan National Institute of Science and Technology (UNIST), Ulsan 44919, Republic of Korea
[*] Author to whom any correspondence should be addressed.

E-mail: kikoo@ulsan.ac.kr

RECEIVED
26 February 2023

REVISED
22 July 2023

ACCEPTED FOR PUBLICATION
1 September 2023

PUBLISHED
22 September 2023

Keywords: inverse-gravity extrusion, double-layered blood vessels, human blood vessels

Supplementary material for this article is available online

Abstract

One of the most promising techniques for treating severe peripheral artery disease is the use of cellular tissue-engineered vascular grafts (TEVGs). This study proposes an inverse-gravity (IG) extrusion technique for creating long double-layered cellular TEVGs with diameters over 3 mm. A three-layered coaxial laminar hydrogel flow in an 8 mm-diameter pipe was realised simply by changing the extrusion direction of the hydrogel from being aligned with the direction of gravity to against it. This technique produced an extruded mixture of human aortic smooth muscle cells (HASMCs) and type-I collagen as a tubular structure with an inner diameter of 3.5 mm. After a 21 day maturation period, the maximal burst pressure, longitudinal breaking force, and circumferential breaking force of the HASMC TEVG were 416 mmHg, 0.69 N, and 0.89 N, respectively. The HASMC TEVG was endothelialised with human umbilical vein endothelial cells to form a tunica intima that simulated human vessels. Besides subcutaneous implantability on mice, the double-layered blood vessels showed a considerably lower adherence of platelets and red blood cells once exposed to heparinised mouse blood and were considered nonhaemolytic. The proposed IG extrusion technique can be applied in various fields requiring multilayered materials with large diameters.

1. Introduction

Large-vessel disease or artery-to-artery embolism accounts for 15%–20% of all ischaemia and strokes [1]. Peripheral artery disease (PAD) is a common circulatory problem in which arteries from heart to brain become narrowed or obstructed by atherosclerosis formed from fibrofatty accumulations on the artery walls [2, 3]. Without treatment, the disease can progress to the point where muscles are starving for oxygen when patients move or even rest [4]. Compared with healthy people, patients with PAD have a lower peak exercise capacity, which limits their physical range of motion [5]. In severe cases of the disease, blood circulation can be so severely reduced that ischaemic muscle damage occurs, potentially resulting in amputation [6].

One well-known treatment for severe PAD is vascular bypass surgery [7], in which donated blood vessels can be used [8]. However, there are limitations to the use of donated blood vessels in this procedure, including donor insufficiency [9] and donor-site morbidity [10]. Consequently, to overcome these issues, synthetic vascular grafts (which are categorised as acellular or cellular) have been developed and clinically utilised [11–13].

Acellular tissue-engineered vascular grafts (TEVGs) are fabricated from biodegradable

polymers, including polyester [14], polytetrafluoroethylene [15], polyglycolic acid [16], poly L-lactic acid [17], and polycaprolactone [18]. However, these grafts are not used when diameters under 6 mm are required owing to the risk of early thrombus calcification and graft occlusion [19–21]. Furthermore, when such acellular grafts are implanted into paediatric patients, the lack of regeneration ability is limiting [22, 23].

In 1998, L'Heureux *et al* developed a cell-sheet-based technique for fabricating cellular TEVGs under 3 mm in diameter [24]. Their cell sheet-based graft withstood a pressure of over 2000 mmHg and prevented the adherence of single platelets in intercellular gaps. Later, this technique was used to produce human-tissue-engineered blood vessels for adult arterial revascularisation [25, 26]. Another technique known as tubular scaffold casting was developed by Meghezi *et al* [27] in which a cylindrical mould was used to cast smooth muscle cells (SMCs) within matrices of type-I collagen. Despite the efficiency of these techniques in the fabrication of cellular TEVGs, the dimensions of the cell sheet or mould limit those of the fabricated grafts, particularly in terms of length. Consequently, this constrains the mass production of such grafts and their application to vessels over 3 mm in diameter, e.g. the radial artery, superior epigastric artery, and lateral circumflex femoral artery; the diameters and lengths of such arteries range from 0.7 to 3.3 mm and 2.2 to 24.7 cm, respectively [28–33]. In recent years, three-dimensional (3D) bioprinting has been utilised to produce large-diameter vascular grafts using biomaterials and living cells [34–37]. Despite its capability to create vessels with branches, this approach can be expensive due to the cost of equipping 3D bioprinters or 3D spotters.

To fabricate long vasculatures with affordable systems in laboratories [38–48], direct extrusion techniques were developed by different research groups. The developed microfluidic devices usually induce coaxial laminar flow and simultaneously encapsulate vascular cells in hydrogels, such as decellularised extracellular matrix [49, 50], type-I collagen [39], calcium alginate [51–53], a mixture of collagen and alginate [50, 54], and customised gelatine methacryloyl (GelMA) [55]. Even though these extrusion techniques have succeeded in formulating long scaffolds, to date, these techniques have reported only under 2 mm-diameter scaffolds with cells [39, 55–57]. In 2020, Qingfei Liang and colleagues [58] increased the viscosity of a mixture comprising GelMA (∼4 wt.%), nanoclay (∼10 wt.%), and N-acryloyl glycinamide (36 wt.%) by 50 million times (10^5 Pa·s at 0.1 s^{-1} shear rate) compared to GelMA (5 wt.%) (0.002 Pa·s at 0.1 s^{-1} shear rate) [59] to directly extrude tubular scaffolds with diameter of approximately 3.5 mm. However, the high stiffness and strong mechanical properties of the extruded scaffolds may make this material unsuitable for cell encapsulation to form the cellular wall of a blood vessel with SMCs [60].

A scaffold over 3 mm in diameter is not produced by simply enlarging the extruding nozzle diameter. When prehydrogel material flows downwards along the gravitational direction, the corresponding flow rate, which is capable of producing a tubular scaffold under 2 mm in diameter, cannot fully fill the enlarged nozzle. As the nozzle diameter increases, the minimum full-filling flow rate should increase. However, the minimum full-filling flow rate in the enlarged nozzle is sufficient to obstruct the laminar flow, which is essential for tubular structure extrusion. In some material cases, the full-filling flow rate can barely maintain the laminar flow. However, this fast velocity results in material wasting and incomplete gelation in the case of photocrosslinking. These are great problems that impede long, large-diameter blood vessel fabrication using extruding techniques.

This study proposes an inverse-gravity (IG) extrusion technique to facilely fabricate long blood vessels exceeding 3 mm in diameter. The method generated coaxial triple-layered scaffolds with outermost sacrificial layers over 8 mm in diameter, as shown in figure 1. To ensure a highly durable vessel, dense human aortic SMCs (HASMCs) were implemented using natural hydrogel (type-I collagen) as a cell-encapsulating material. The long gelation time of collagen required the employment of calcium alginate in the outermost layer and the core layer as a supporting material. Following collagen gelation, the supporting layers of alginate were removed. Then, human umbilical vein endothelial cells (HUVECs) were seeded as tunica intima on the inner surfaces of the HASMC scaffolds. The mechanical properties, haemocompatibility, and subcutaneous implantability of the double-layered vessel were measured and evaluated. The experimental results confirming the advantages of the IG technique were double-checked both theoretically and numerically.

2. Theory and design

To replicate the multilayered structure of human blood vessels, an extruding device is required to generate coaxial laminar flow. It is well known that laminar flow occurs under a Reynolds number (*Re*) of 2100 [61]. The *Re* proportionately depends on the density ρ, flow speed V, characteristic linear dimension of fluid flow D (nozzle diameter), and inverse of viscosity $1/\mu$, [62] as described in equation (1):

$$Re = \frac{\rho V D}{\mu}. \tag{1}$$

The density and viscosity are usually determined by the prehydrogel material properties so that as the

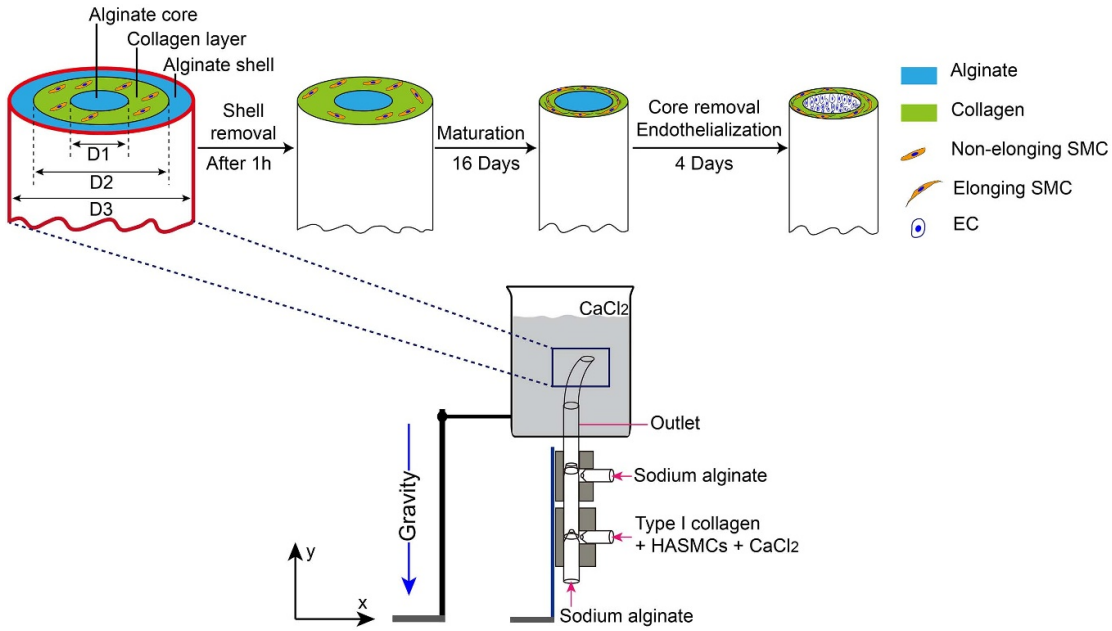

Figure 1. Conceptual visualisation of the double-layered blood vessel extruder. A triple-coaxial laminar flow device is assembled under a $CaCl_2$ beaker. A hole is drilled in the base of the beaker and connected to the outlet tube of the extrusion device. Sodium alginate (1.5% w/v) is introduced via the bottom inlet as the core and via the upper inlet as a shell layer. Type-I collagen containing HASMCs and $CaCl_2$ is pumped into the middle inlet. The collagen layer is trapped between the alginate shell layer and the alginate core, where it becomes a hydrogel. The extruded scaffold is then immersed in prewarmed $CaCl_2$ (20 mM, 37 °C) for 45 min to ensure complete gelation. Afterwards, the alginate shell is removed after a 24 h incubation period in HASMC media. The alginate core functions as a mandrel to maintain the tubular shape of the collagen layer during scaffold maturation. After a 16 day incubation period, the mandrel is removed. Finally, the HASMC scaffold is endothelialised with HUVECs after a 16 day maturation period.

nozzle diameter increases, the flow velocity should be reduced to maintain *Re*.

When a fluid flows along the gravitational direction inside a circular nozzle, some of the fluid flows along the wall and experiences friction force from the inner surface. This friction force makes the fluid flowing near the wall slow down. The friction depends on the viscosity, density, and pressure of the fluid. As the nozzle diameter increases with the same initial flow velocity (i.e. the same initial pressure), the effect of the wall surface friction on the velocity of the fluid far from the wall decreases. Over a certain diameter, the velocity of the fluid far from the wall is accelerated by gravitational force with little effect from the friction force of the wall surface. This acceleration causes the fluid far from the wall to flow not in parallel with the fluid near the wall, leading to a chaotic stream so that the fluid cannot fully fill the nozzle to the end. Therefore, as the nozzle diameter D increases, the initial flow velocity should increase to fully fill the inside of the nozzle (denoted hereafter as the full-filling velocity).

As discussed above, the increased full-filling velocity of the fluid in the enlarged nozzle along the gravitational direction is contradictory to extruding coaxial tubular scaffolds. However, the IG extrusion technique is not hindered by gravity in the full-filling of the nozzle. In contrast, gravity contributes to slowing down the fluid, resulting in the full-filling of the nozzle in the inverse gravitational direction. Therefore, any nozzle can be fully filled with any fluid at any initial velocity. Using an 8 mm-diameter nozzle, these two methods were compared numerically, as shown in figure 2. In the gravitational direction, 300 ml min^{-1} of water from a perpendicular inlet barely fully filled the nozzle (figure 2(a)). In contrast, 3 ml min^{-1} of water in the inverse gravitational direction fully filled the nozzle (figure 2(b)).

The 1.5% w/v alginate and 10 mg ml^{-1} type-I collagen along the gravitational direction could not fully fill the 8 mm-diameter nozzle at 3.0 ml min^{-1} and 1.5 ml min^{-1} flow rates, respectively, as shown in figure 3(a)). However, the proposed method fully filled the 8 mm-diameter nozzle and extruded a coaxial double-layered hydrogel at the same fluid velocities (figures 3(b) and (c)). Another double-layered scaffold from the 10 mm-diameter nozzle (figure 3(d)), triple-layered scaffold from the 8 mm-diameter nozzle (figure 3(e)), and quadruple-layered scaffold from the 8 mm-diameter nozzle (figure 3(f)) were extruded along the inverse gravitational direction. In the gravitational direction, the maximum flow rate (65 ml min^{-1} alginate and collagen) of our syringe pump (Pump 11 Elite, Harvard Apparatus, USA) cannot fully fill the 8 mm-diameter nozzle of the double-layer extruding device (figure S2).

Using the IG extrusion technique, this study successfully fabricated a coaxially layered HASMC and

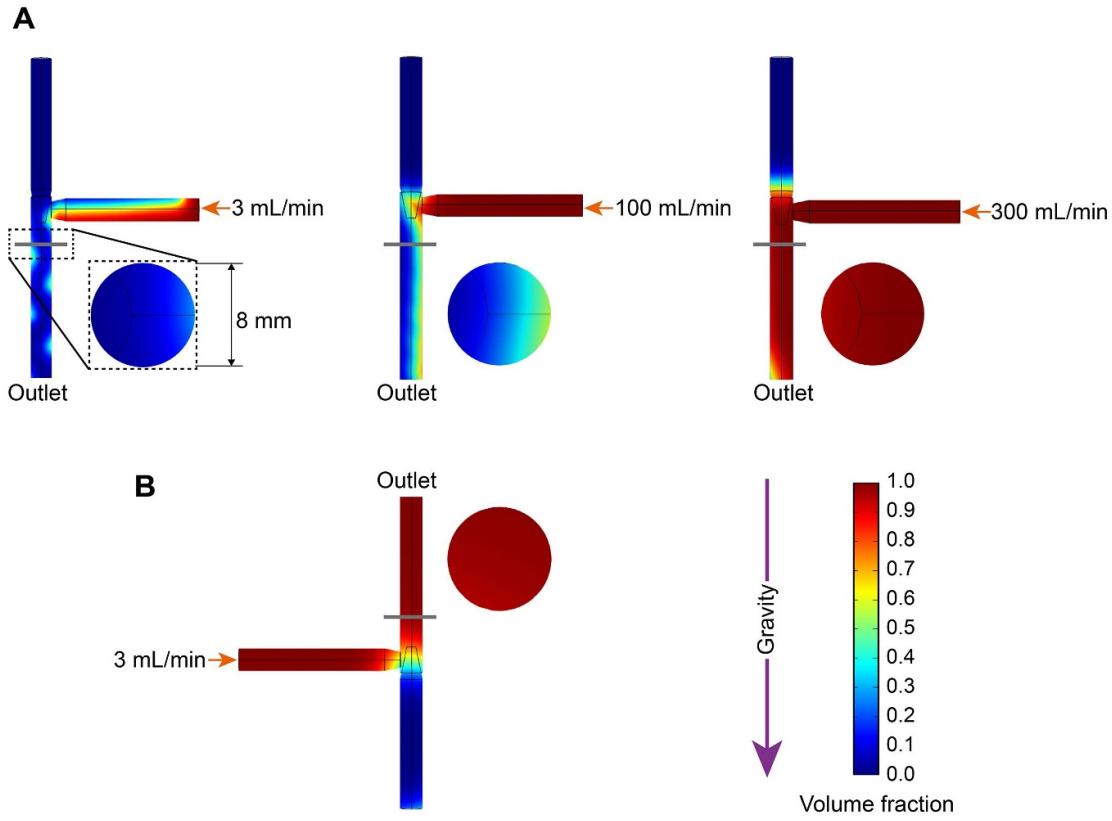

Figure 2. Simulation of water filling into the main pipe via a single-branched inlet. The volume fraction contours of the liquid/air in the geometry are shown in this figure. The circle insets are the cross-sections of the pipe at 10 mm from the branched inlet. (a) Three ml min^{-1} and 100 ml min^{-1} flow rates of water along the gravitational direction cannot fully fill the 8 mm-diameter nozzle. The 300 ml min^{-1} flow rate of water can fully fill the pipe. (b) Three ml min^{-1} flow rate of water along the inverse gravitational direction fully fills the 8 mm-diameter nozzle.

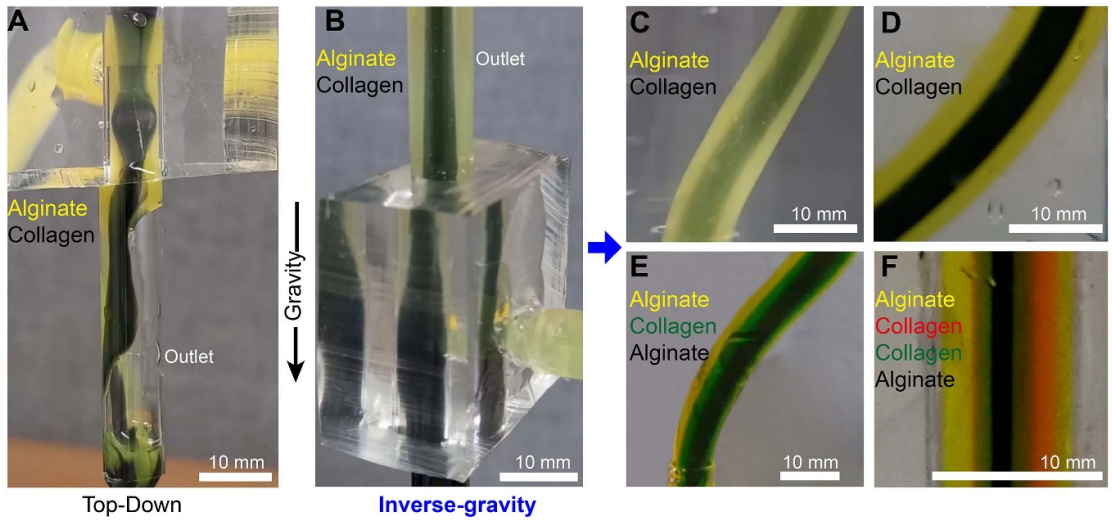

Figure 3. Coaxial laminar scaffold formation using alginate and collagen. (a) One and a half ml min^{-1} flow rate of yellow alginate and 3.0 ml min^{-1} flow rate of black collagen cannot fully fill the nozzle along the gravitational direction. (b) One and a half ml min^{-1} flow rate of yellow alginate and 3.0 ml min^{-1} flow rate of black collagen along the inverse gravitational direction can fully fill the nozzle and form a coaxial laminar flow. (c) Double-layered scaffold extruded out of the 8 mm-diameter nozzle. (d) Double-layered scaffold extruded out of the 10 mm-diameter nozzle by IG extrusion. (e) Triple-layered scaffold and (f) the quadruple-layered scaffold prepared by IG extrusion.

HUVEC scaffold with a diameter exceeding 3 mm, as shown in figure 1. To support the tubular structure of the collagen and HASMC mixture during the gelation of collagen, calcium alginate was layered both inside and outside of the HASMC layer. After the supporting calcium alginate layers were removed, HUVECs

were seeded on the inner surface of the HASMC structure.

3. Results and discussion

3.1. Pure type-I collagen as a scaffold material

To fabricate the scaffold, this study used type-I collagen as a bioink. Type-I collagen has been widely used in the fields of tissue engineering and regenerative medicine because of its immunogenicity, rapid gelation, biocompatibility, fibrous structure, and biodegradability [63, 64]. Additionally, it possesses specific peptide sequences that can be recognised by cell surface receptors as substrates for cell adhesion and migration. Consequently, type-I collagen has been used as a powerful coating material for cell-culture applications [65, 66]. Furthermore, the stiffness of type-I collagen is higher than that of fibrin and Matrigel at the same concentration [67, 68].

In the authors' previous report, a HUVEC–HASMC vessel with a diameter of approximately 600 μm was extruded using a mixture of 3 mg ml^{-1} type-I collagen (25%) and 1.8% w/v sodium alginate (75%) [54]. The long gelation time of type-I collagen (10–30 min) [69] requires it to be mixed with sodium alginate for rapid gelation before the collapse of its lumen structure. In the present study, the IG technique enabled the collagen concentration to be increased from 3 to 10 mg ml^{-1} to enhance both cell proliferation and the mechanical properties of the scaffold [68]. As expected, cell proliferation with 10 mg ml^{-1} pure collagen was superior to that with mixtures of 25% 10 mg ml^{-1} collagen and 75% 1.8% w/v sodium alginate (figure S3).

In figure S3(a), the magnified images reveal that the collagen gel contained many distinguishable fibrils, while the collagen–alginate mixture appeared almost monolithic. As shown in figure S3(b), the highly fibrous microstructure of the pure collagen hydrogel made it more conducive to cell spreading, migration, and proliferation than the mixture. Most HASMCs appeared to be spheroidal in shape and slowly doubled in the hydrogel mixture, while the cells in the pure collagen membrane spread well, quickly increasing their population over the same 3 day timescale.

3.2. Tuneable dimensions of the extruded scaffold

Figure 4(a) shows a triple-layered cell-free scaffold during formation in a $CaCl_2$ beaker; the light-yellowish outermost layer is calcium alginate, the green middle layer is type-I collagen, and the black innermost layer is the calcium alginate core. Variations in the inlet flow speed affected both the diameters and thicknesses of every layer (figures 4(b) and (c)). As the flow speed of the collagen increased from 1 to 3 ml min^{-1}, the thickness of the collagen layer increased from 0.85 to 2.38 mm; however, the inner diameter of the vessel decreased from 3.38 to 2.29 mm (figure 4(b)). As the flow speed of the alginate core increased from 0.5 to 1.5 ml min^{-1}, the inner diameter of the vessel increased from 2.49 to 4.19 mm, although the thickness of the collagen layer decreased from 1.38 to 1.07 mm (figure 4(c)). It is considered that an increase in the flow speed of one material increases its area but reduces the area of neighbouring materials in the gelated scaffold. However, these tendencies showed no direct proportionality.

Figures 4(d) and S13(a) show a triple-layered cell-free scaffold after gelation. Figures 4(d)–(f) and S13(b)–(d) show images of the alginate-removed scaffolds after incubation for 1 h at 37 °C since the extrusion. The inner and outer diameters of the cell-free scaffold were approximately 5.2 mm and 3.5 mm, respectively (figure 4(e)). After a maturation period of 2 d, the length of the HASMC-laden scaffold was approximately 26 cm (figure 4(f)).

3.3. Morphology of the matured HASMC vessels

The 16 day-matured HASMC vessels were analysed histologically to investigate their cross-sectional cell morphology, as shown in figure 5. The vessel thickness of the pure 10 mg ml^{-1} collagen scaffold declined from 227 μm on day 2 to 64 μm on day 16 (figures 5(a) and (b)). However, the vessel thickness of the scaffold containing 25% 10 mg ml^{-1} collagen and 75% 1.8% w/v sodium alginate remained consistent (at approximately 600 μm) up to day 16 (figure 5(b)). As the HASMCs in the pure collagen scaffold matured, they became elongated; this decreased the ratio of the circle-shaped cells from 60.5% on day 2 to under 10% on day 16 (figure 5(c)). However, the circle-shaped HASMCs in the mixed scaffold maintained a ratio of approximately 80% during maturation (figure 5(c)).

The matured HASMCs demonstrated elongated cell nuclei orientations that differed according to the scaffold material. The orientation of the major axis (longer part) was measured for all the elongated HASMC nuclei in one 100 × 100 μm histological image. Based on the measured elongated orientation, the standard deviation (SD) was measured to assess how the matured HASMCs elongated in a similar direction. As shown in figure 5(d)), the SD of the elongated cell nuclei orientation in the pure collagen scaffold decreased from 23.2° on day 2 to under 5° on day 16. The SD of the elongated cell nuclei orientation in the mixed scaffold was maintained at approximately 40° (figure 5(d)). Accordingly, during maturation, the HASMCs in the pure collagen scaffold elongated in a similar direction, which was considerably different from those in the mixed scaffold. The elongated orientation was supposed to be the circumferential direction of the HASMC vessel cross-section.

There was considerably more HASMC elongation and proliferation activity with pure collagen

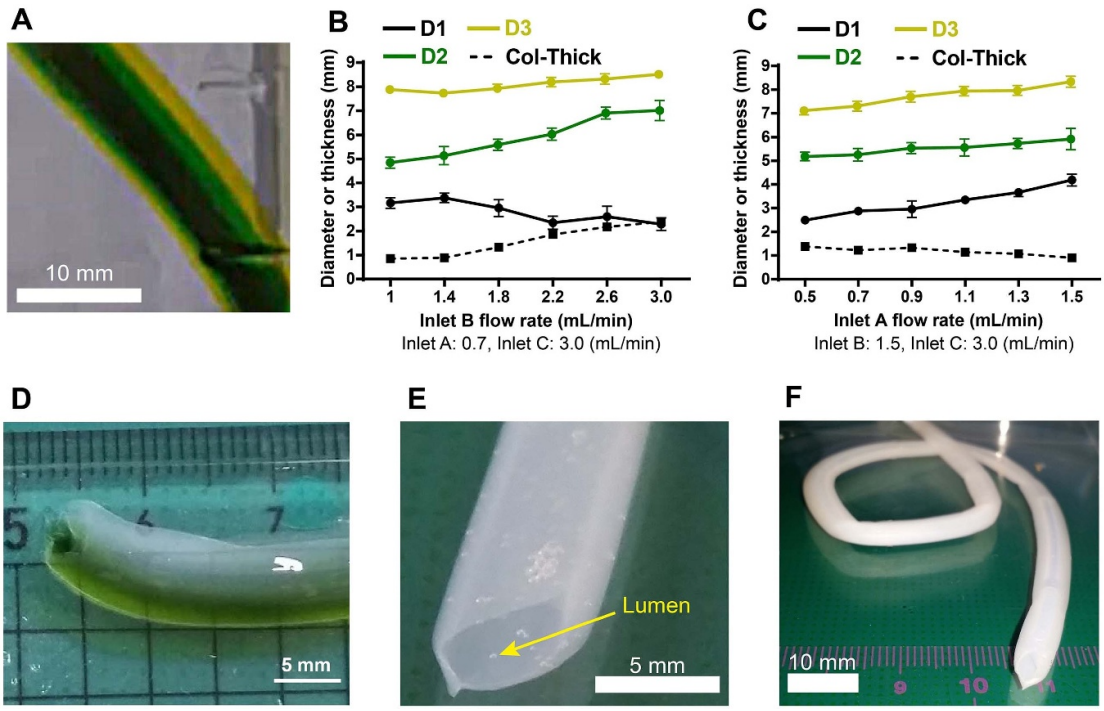

Figure 4. Triple-layered scaffold. (a) Triple-layered scaffold in a $CaCl_2$ beaker during formation; the light yellow outermost layer is calcium alginate, the green middle layer is type-I collagen, and the innermost black layer is the calcium alginate core. (b) Graph showing the layer diameter and thickness according to the collagen flow rate from 1 to 3 ml min^{-1} (sample size $n = 6$ from three experiments). (c) Graph showing the layer diameter and thickness according to the alginate core flow rate from 0.5 to 1.5 ml min^{-1} (sample size $n = 6$ from three experiments). (d) Triple-layered cell-free scaffold after extrusion. (e) Alginate-removed cell-free scaffold with a lumen of approximately 3.5 mm in diameter formulated after incubation for 1 h at 37 °C following extrusion. (f) Alginate-removed HASMC-laden scaffold after a 2 day maturation period with a length of 26 cm.

than with 25% collagen and 75% alginate on the 3D culture inside the scaffold (figure 5(a)) and on the two-dimensional culture (figure 3S(b)). The authors' previous study also reported this difference [54]. Sodium alginate is known not to be degraded enzymatically by animal cells [70] or to have no polymeric backbone for cell binding [71]. Consequently, the low HASMC activity is believed to be due to the properties of alginate.

Figure 5(e) presents a cross-section of the mature HASMC pure collagen scaffold stained with α-smooth muscle actin (green) and 4',6-diamidino-2-phenylindole (DAPI) (blue) on day 16. The thickest and thinnest parts of the vessel wall were 95 and 22.4 μm (figure 5(e)), respectively. Averagely, the thickest wall measured 92.37 $\pm$ 6.91 μm while the thinnest wall measured 24.69 $\pm$ 5.82 μm after 16 d of maturation. It is believed that this difference originated from the nonsymmetrical collagen laminar flow (green, orange) in the main pipe of the extruder (figures 3(e) and (f)). According to another numerical analysis (figure S6), a slight angle change of the inner glass pipe in the proposed device could disrupt the symmetry of the laminar flow layer thickness. Our manual fabrication process of the proposed device was supposed to result in a difference in the thickness of the matured HASMC vessel. In order to improve wall thickness uniformity, we tested a 3D-printed device (FormLabs Form 2, FormLabs, USA) as shown in figure S10. The 3D-printed device has the same design concept with the manually fabricated device but was 3D-printed for the precise layering. The uniformity of the middle and outer layer has been much more improved with the 3D-printed device. It looks to solve the non-coaxial issue.

3.4. Mechanical properties of the matured HASMC vessels

The mechanical properties of the matured HASMC vessels were evaluated by measuring the maximal values of the burst pressure, longitudinal breaking force, and circumferential breaking force applied to the scaffolds (figure 6). These measurements were obtained inside a deionised water reservoir at approximately 37 °C, and the results revealed similar trends (figures 6(c), (f) and (i)). Longer maturation periods and higher collagen concentrations of the pure collagen scaffold resulted in a higher durability. The burst pressure, longitudinal breaking force, and circumferential breaking force of the 10 mg ml^{-1} collagen vessel were measured to be 416 mmHg, 0.69 N, and 0.89 N, respectively, on day 21. However, the mixed scaffold became progressively weaker during culture; on days 10, 16, and 21, the vessels were so fragile that they broke when they were fixed to the measuring

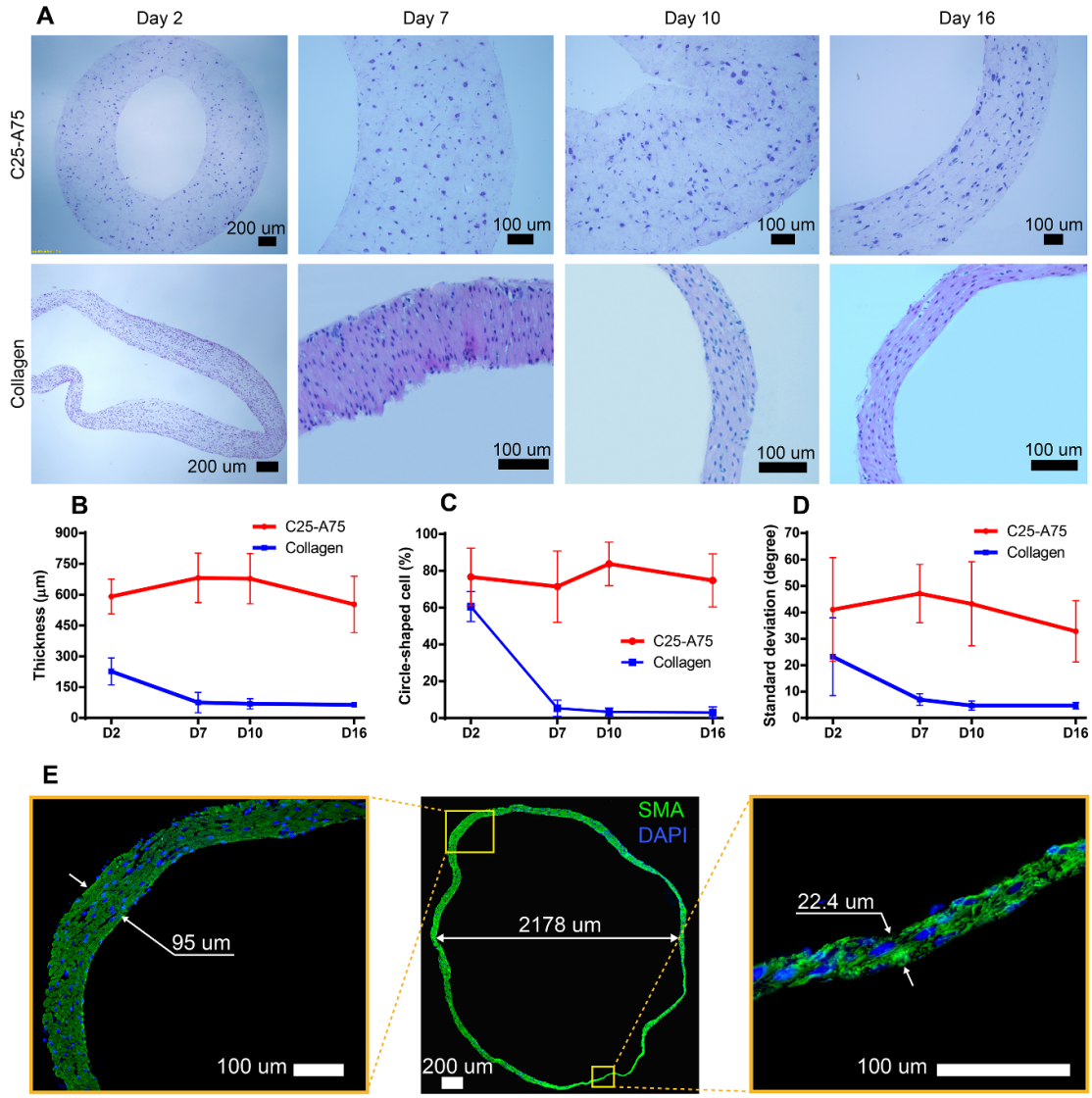

Figure 5. Histological analysis. (a) H&E-stained circumferential cross-sections of the two scaffold types on days 2, 7, 10, and 16 (sample size $n = 5$ from two experiments). (b) Scaffold wall thickness, as cultured (sample size $n = 5$ from two experiments). (c) Circle-shaped cell ratio, as cultured (sample size $n = 5$ from two experiments). (d) Standard deviation (SD) of the elongated orientation of the cultured cells (sample size $n = 5$ from two experiments). (e) Cross-section of the collagen scaffold with smooth muscle actin (SMA) (green) and DAPI (blue) staining at day 16.

tool. In terms of longitudinal breaking force, it was impossible to measure the mixed vessel after day 7.

The highest burst pressure of 416 mmHg is comparable to the burst pressure of native human blood vessels (170–630 mmHg) with a diameter between 1.6 and 5 mm [72, 73]. However, the durability recorded in the present study was far below the 2100 mmHg reported by L'Heureux *et al* [24] Nonetheless, considering the 9 week maturation period and the thickness of the wall (approximately 1500 μm), the durability of the vessel in the present study could be improved. One option for improving the durability and other functionalities is to layer human fibroblasts out of the HASMC layer as tunica externa. According to previous reports, human fibroblasts cocultured as tunica externa anchored artificial vessels to host tissues after implantation [24, 74, 75] and enhanced their mechanical durability by secreting and rearranging newly produced extracellular matrix [76, 77].

The low durability could be attributed to the uneven thickness of the extruded vessel wall. A burst usually initiates from the weakest point; consequently, the thinnest point of the wall is suspected to have broken at low pressure even though the other thicker wall could have withstood higher pressure. As discussed above, if the inner pipe of our device was positioned more accurately, the uniformity of the wall thickness could be improved, which is expected to enhance the durability of our vessel.

3.5. Seeding endothelial cells

In accordance with the methods of L'Heureux and Meghezi, [24, 27] HUVECs were seeded on the inner surfaces of 16 day-old HASMC collagen vessels. Two

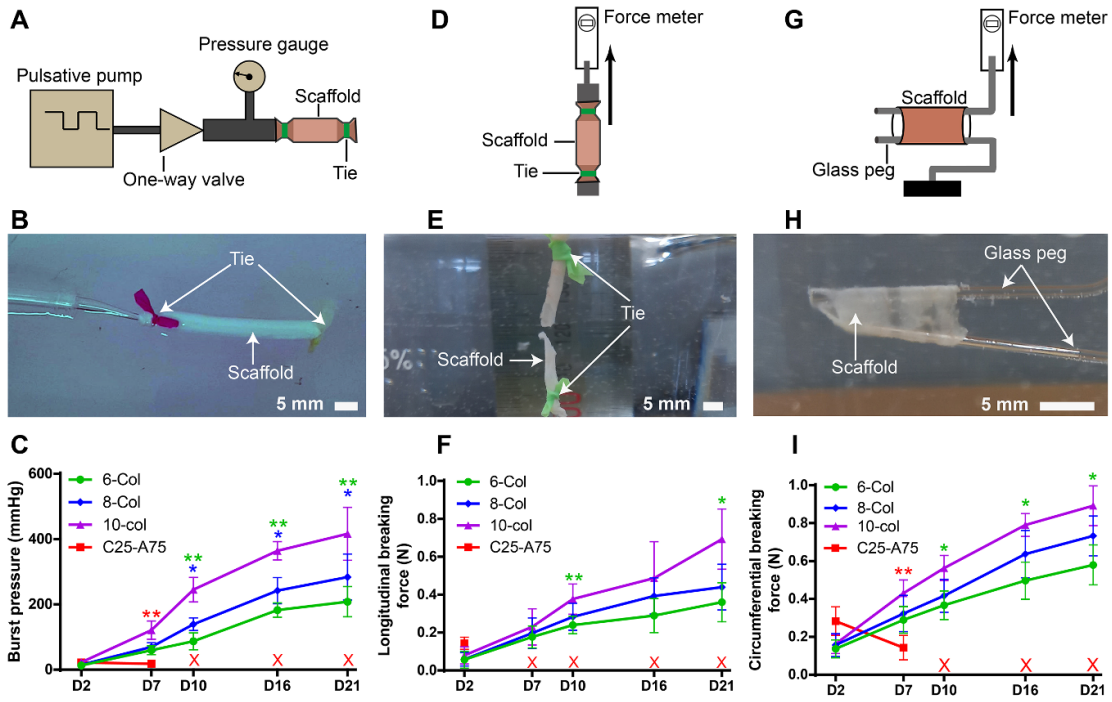

Figure 6. Mechanical properties of the cell-laden scaffolds. (a) Conceptual schematic of the burst pressure durability measuring system. (b) Burst pressure measurement of the HASMC collagen scaffold after 16 d of maturation. (c) Graph showing the burst durability over 16 d. (* and ** indicate $0.01 < p < 0.05$ and $0.001 < p < 0.01$, respectively, comparing 10-col to 6-col, 8-col, and C25–A75; sample size $n = 3$ from two experiments.) (d) Conceptual schematic of the longitudinal breaking force measuring system. (e) Longitudinal breaking force measurement of the HASMC collagen scaffold. (f) Graph showing the longitudinal durability over 16 d. (* and ** indicate $0.01 < p < 0.05$ and $0.001 < p < 0.01$, respectively, comparing 10-col to 6-col, 8-col, and C25–A75; sample size $n = 3$ from three experiments.) (g) Conceptual schematic of the circumferential breaking force measuring system. (h) Circumferential breaking force measurement of HASMC collagen (1 cm in length). (i) Graph showing circumferential durability over 16 d. (* and ** indicate $0.01 < p < 0.05$ and $0.001 < p < 0.01$, respectively, comparing 10-col to 6-col, 8-col, and C25–A75; sample size $n = 3$ from three experiments.).

days after seeding, the HUVEC confluency on both scaffolds was approximately 22%. However, for the collagen vessel, this increased up to 82% after two additional days of maturation, while the value for the mixed vessel reached approximately 40% (figures 7(a) and (b)).

Figure 7(c) presents a cross-sectional view of the endothelialised vessel 4 d after endothelial cell seeding. After endothelialisation, the average outer and inner diameters of the vessels were approximately 2.57 mm and 2.38 mm, respectively. HUVECs (red) formed a well-attached monolayer on the inner surface of the HASMC wall-like structure (green). These HUVEC–HASMC double layers imitated the tunica intima and tunica media of native human blood vessels. The thickness of the HUVEC monolayer varied between 8 and 17 μm. According to previous research, higher HUVEC seeding densities [27] and supplementary angiogenic growth factors (GFs), such as basic fibroblast GF [27, 78, 79], hepatocyte GF [80], and vascular endothelial GF [79], could enhance both HUVEC growth and confluency.

In the authors' previous work, the HUVEC–HASMC vessel exhibited significantly higher durability (approximately 0.02 N) on day 20 after extrusion compared with the HASMC-only vessel (approximately 0.015 N) despite, the embedding material containing 25% collagen and 75% alginate [54]. Therefore, in-depth investigations into the effects of HUVEC layers on the mechanical durability of pure collagen vessels are needed.

Figures 7(d) and (e) show the platelets and red blood cells (RBCs) on the inner surface of the vessel without and with HUVECs in 10 mg ml^{-1} pure collagen. The numbers of platelets and RBCs were found to be at least one-third lower on the HUVEC vessel surface than on the HUVEC-less vessel surface (figures 7(f) and (g)). Endothelial cells possess antithrombotic activity by releasing nitric oxide and prostacyclin, both potent vasodilators and inhibitors of platelet aggregation [81]. L'Heureux *et al* demonstrated that a vessel with 99.2% confluent endothelial cells on a luminal surface increased the expression of prostacyclin threefold since they responded to thrombin stimulation [24]. Indeed, the presence of endothelial cells on the inner surface of tissue-engineered blood vessels increased the patency rates of implanted small-diameter synthetic vascular grafts in the human body [82–84].

Herein, the haemocompatibility of mature vessels was evaluated in terms of haemolysis using mouse blood (figure 7(h)). The incubation of diluted RBCs

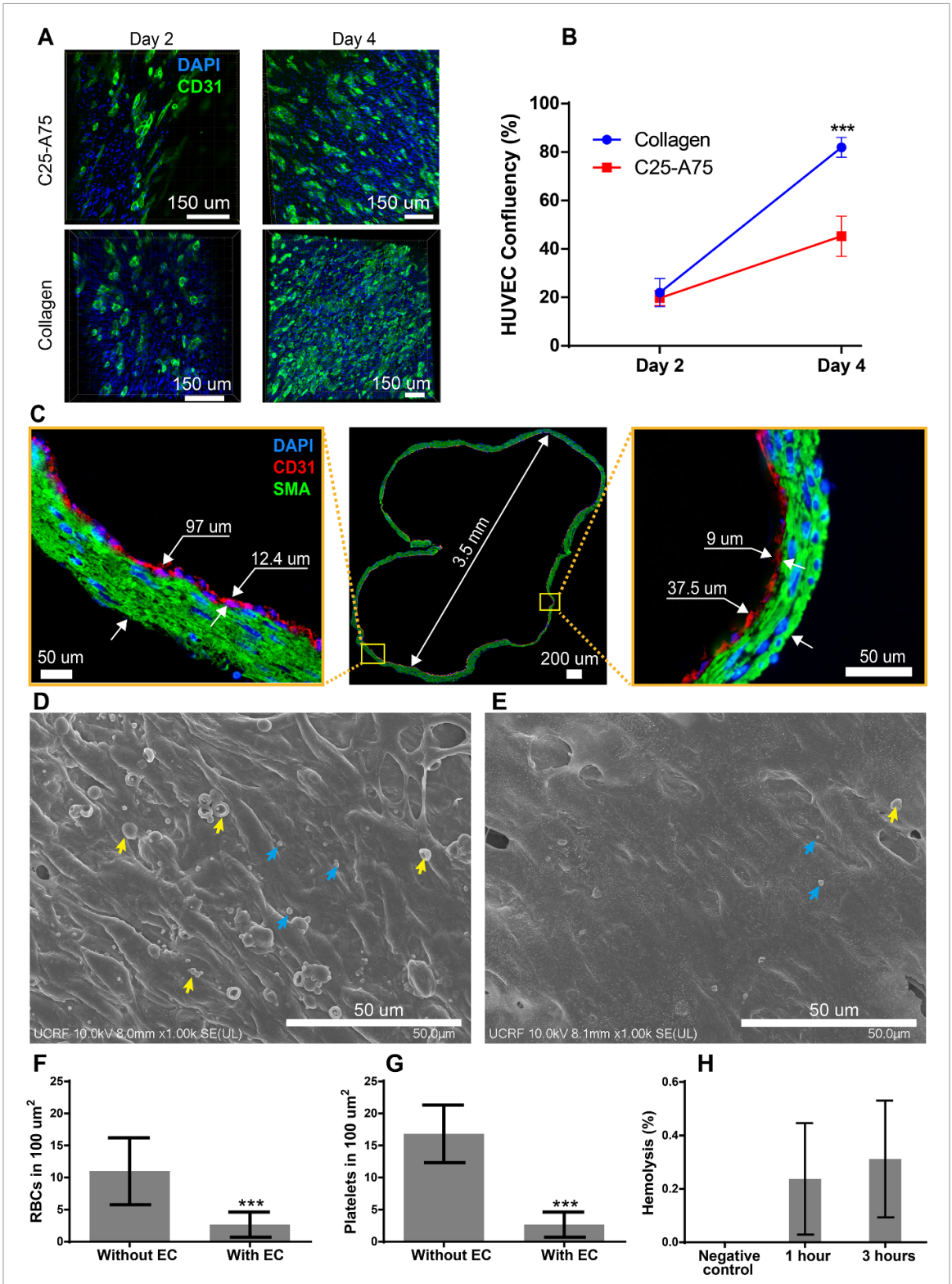

Figure 7. Endothelialisation on the inner surfaces of 16 day-old HASMC collagen vessels. (a) Stained HUVECs (green) on the inner surfaces of the HASMC vessels. (b) HUVEC confluency on day 2 and day 4 after HUVEC seeding. (*** indicates $p < 0.001$ compared with the mixture scaffold; sample size $n = 5$ from two experiments). (c) Cross-section of the double-layered scaffold with SMA (green), DAPI (blue), and CD31 (red) staining after 4 d of endothelialisation. (d), (e) SEM images of adhered platelets and red blood cells (RBCs) on the inner surfaces of the vessels (d) without and (e) with HUVECs. The blue arrows indicate platelets. The yellow arrows indicate RBCs. (f) RBCs attached to the 100 μm^2 inner surface of the vessels without and with HUVECs. (*** indicates $0.001 > p$; sample size $n = 6$). (g) Platelets attached on the 100 μm^2 inner surfaces of the vessels without and with HUVECs. (*** indicates $0.001 > p$; sample size $n = 6$). (h) Haemolysis percentage over time.

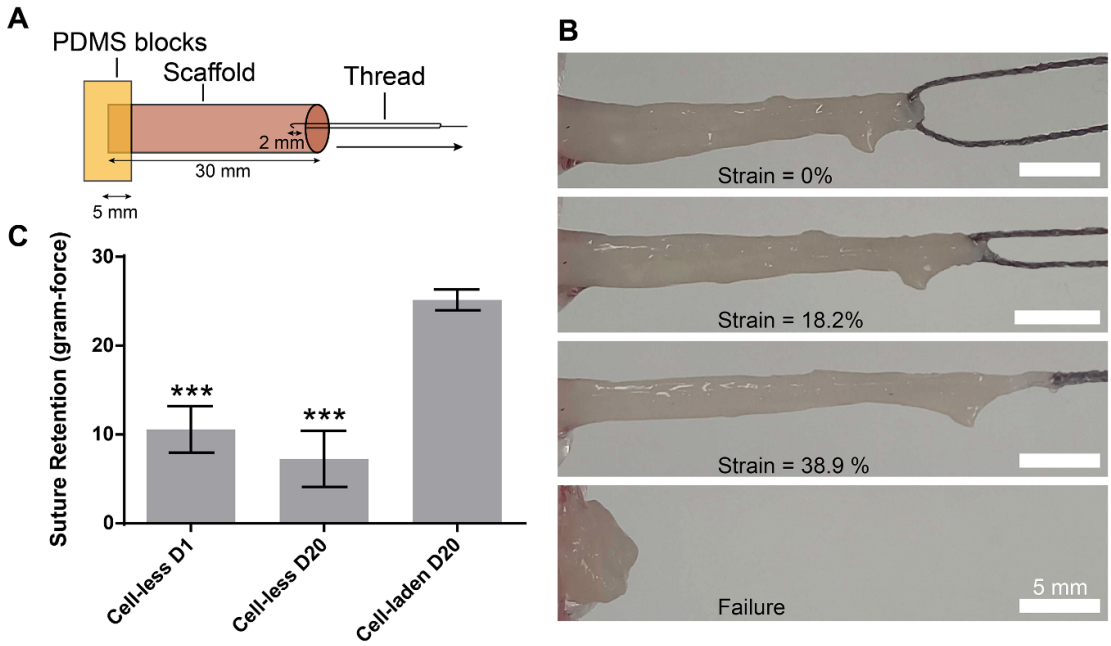

Figure 8. Suture retention strength of the endothelialised vessels. (a) Conceptual sketch of the measuring configuration. (b) Vessel during the suture strength measuring experiment (pure collagen 10 mg ml^{-1}, 4 d after endothelialisation). (c) Suture retention force comparison between the cell-less scaffold and the cell-laden scaffold at day 1 and day 20. (*** indicates $p < 0.001$; sample number $n \geqslant 3$ from two experiments.)

with the HUVEC vessel for 1 h and 3 h exhibited a haemolytic ratio of less than 0.6%, which was considered nonhaemolytic according to ISO/TR 7406.

3.6. Suture retention strength of the endothelialised vessel

We measured the suture strength of the mature vessel (pure collagen 10 mg ml^{-1}, 4 d after endothelialisation) using a lab-made system (figure 8(a)). The mature vessel retained almost three times higher strength than the cell-less scaffold at day 20 (figure 8(c)). This result was consistent with empirical data from other groups [85–87]. Increasing the maturation time, wall thickness, and wall uniformity of the vessel could enhance the suture retention force.

3.7. Subcutaneous implantation

A subcutaneous implantation experiment was performed to test the vessel biocompatibility *in vivo*. Considering the mouse size, a 1 mm diameter vessel was extruded using the proposed IG method and another triple-layer device with smaller-diameter glass capillaries (0.58 mm inner diameter for the inlets, 1.5 mm for the middle pipe, 1.8 mm for the outlet) (figure S14). Approximately 0.015 N were seeded on the luminal surface and then cultured for 4 d. Once matured, the outer diameter of the vessel was about 1 mm and the inner diameter was measured at approximately 0.82 mm (video S6). The endothelialised vessel was then subcutaneously implanted under the dorsal skin of a mouse (figures 9(a) and (b)). For 14 d after the implantation surgery, the host mouse exhibited healthy activity, no fever, and no infection (figure 9(c)). On the 14th day of the implantation surgery, the implanted vessel was harvested, cross-sectioned, and then stained (figures 9(d) and (e)). The harvested tissue showed that the implanted vessel was well planted in the surroundings.

4. Conclusion

This study used the IG extrusion technique to demonstrate a HUVEC–HASMC double-layer vessel, which was embedded initially inside a high-concentration scaffold of pure collagen. The conventional limitations of achieving coaxial laminar flow in large-diameter nozzles were overcome by the simple reversal of the extrusion direction, which caused gravity to aid the formation of laminar flow rather than hinder it. It is expected that the proposed technique could be used in various fields to generate more than just tubular structures, which could be one step forwards in developing the extrusion method. The procedure presented in this study can still be improved to enhance the vessel characteristics up to the clinical level, including higher initial cell density, longer maturation time, higher collagen concentration, and modification of the extruder. Currently, the authors are focusing on multicell coculturing in multilayered hydrogels using the IG extrusion technique.

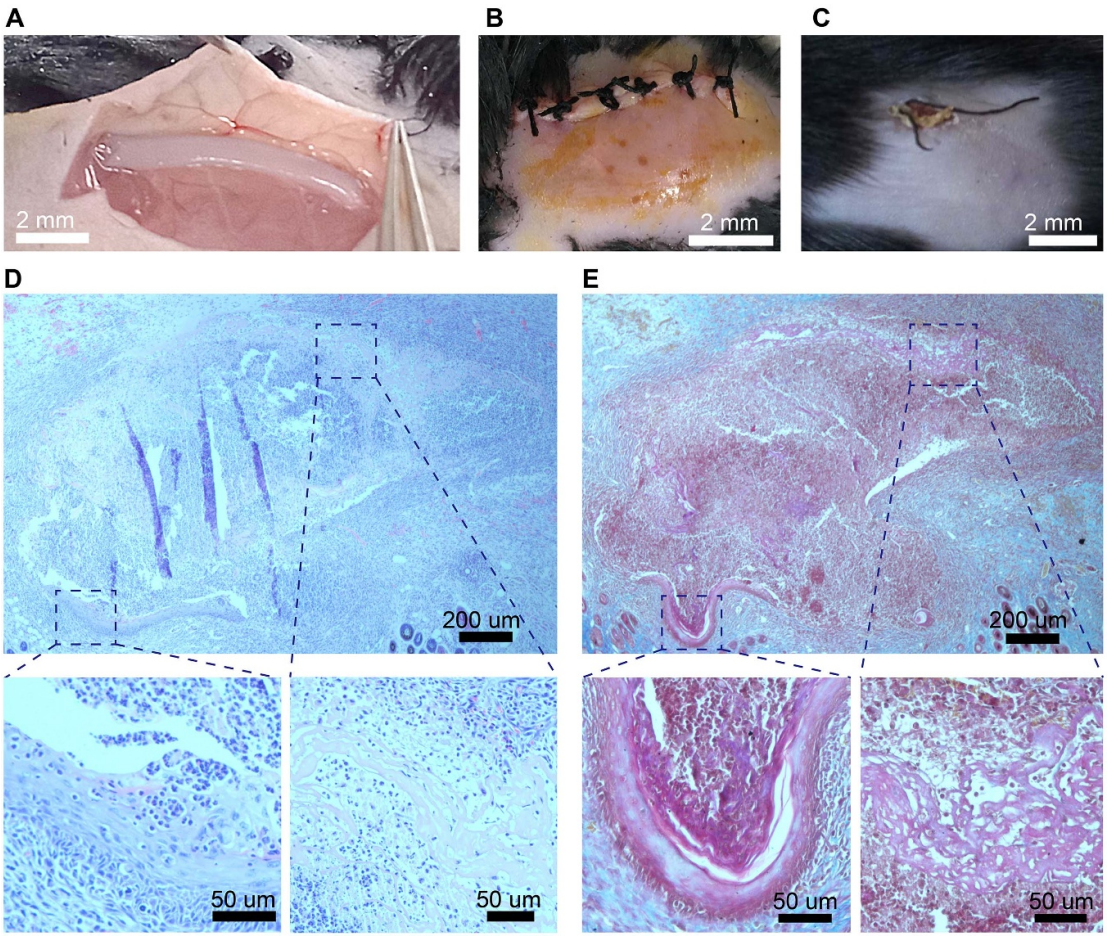

Figure 9. Subcutaneous implantation. (a) Vessel implanted beneath the mouse dorsal skin. (b) Dorsal skin after suturing. (c) Dorsal skin 14 d after implantation. (d) Cross-section of the implanted vessel harvested 14 d after the surgery and stained with haematoxylin and eosin. (e) Cross-section of the implanted vessel harvested 14 d after the surgery and stained with Masson's trichrome stain.

5. Experimental section

5.1. Simulation

COMSOL Multiphysics (version 5.6, COMSOL, USA) software was used to perform 3D numerical simulations for a double-coaxial laminar flow device. The geometry and fluid parameters for the simulation were defined as shown in figure S4. Navier–Stokes equations [88] were used as the governing equations for our simulation (equation (2)).

$$\rho\frac{\mathrm{d}\vec{V}}{\mathrm{d}t} = \rho\vec{g} - \nabla p + \mu\nabla^2\vec{V} \tag{2}$$

where V is the flow velocity, t is time, ρ is density, μ is viscosity, p is pressure, and g is gravity ($g = 9.8\ \mathrm{m\,s^{-2}}$).

5.2. Extrusion device

Based on the authors' previous studies [51, 54], a double-coaxial flow device was fabricated to test the formation of coaxial laminar scaffolds. The device comprised two inlets and one outlet made from glass Pasteur pipettes (approximately ∅ 8 mm) and serological pipettes (∅ 10 mm). The inlets had tapered ends that were partially inserted into the outlet for coaxial assembly (figure 10(a)). Polydimethylsiloxane (PDMS) was used to ensure the integrity of the inlets and outlet.

Based on the double-coaxial laminar flow device, triple- and quadruple-coaxial laminar flow devices were further developed to directly extrude multilayered scaffolds for the fabrication of double-layered blood vessels over 3 mm in diameter. The triple device comprised five glass tubes with three inlets, one link, and one outlet (figure 10(b)). The quadruple device comprised seven glass tubes with four inlets, two links, and one outlet (figure 10(c)). The glass tubes were approximately 8 mm in diameter. One end of the inlet and the links were tapered to narrower than 5.5 mm, and the tapered tubes were partly inserted into the links and the outlet, as shown in figures 1 and 10(b), (c). All glass tubes were assembled tightly using cuboid-shaped PDMS bodies. The fabricated devices were autoclaved carefully before the cell experiments.

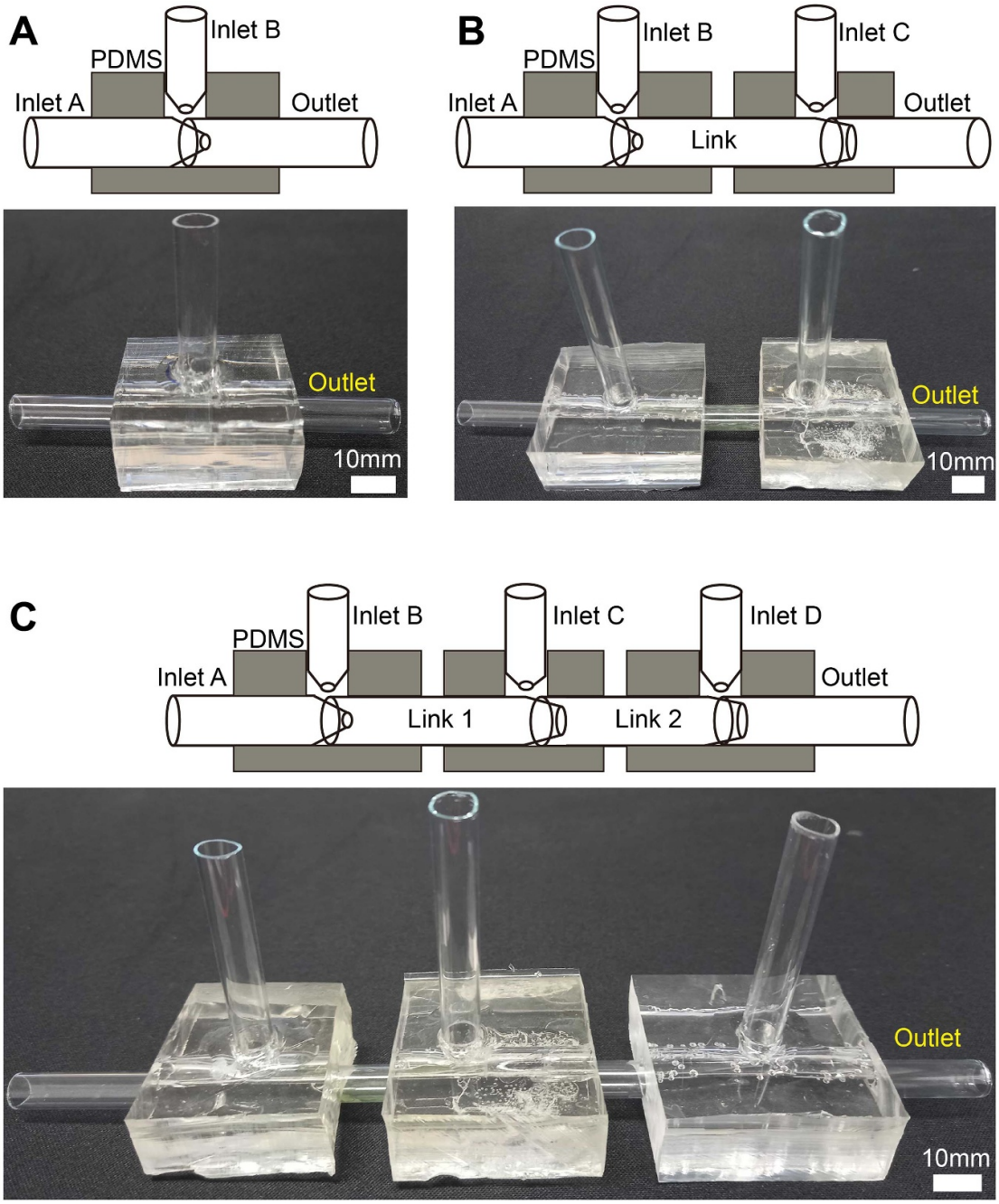

Figure 10. Extruding devices. (a) Schematic sketch and picture of the double-layer device. (b) Schematic sketch and picture of the triple-layer device. (c) Schematic sketch and picture of the quadruple-layer device.

5.3. Hydrogel preparation

Sterile sodium alginate solution was obtained according to a previously reported method [54]. Sodium alginate powder (13035S1201, JUNSEI, Japan) was dissolved in deionised water to obtain a 0.5% w/v solution before being vacuum filtered using a 0.22 μm bottle-top filter (J1.F204.500, SCI-lab, Republic of Korea) in a clean laminar flow hood. The filtered sodium alginate was frozen overnight at −80 °C before being lyophilised for a minimum of 72 h. The lyophilised alginate powder was dissolved in 1× phosphate-buffered saline (PBS) (14190250, Thermo Scientific, USA) without $CaCl_2$ and magnesium chloride ($MgCl_2$) at 1.5% w/v.

Type-I collagen solution was obtained following a video protocol published by AIM Biotech (Singapore) [89]. Briefly, a bovine type-I collagen solution (TeloCol®-10, 5226, Advanced BioMatrix, USA) was kept on ice and neutralised using 0.5 N sodium hydroxide (NaOH) (MFCD00003548, Life Science, Republic of Korea) supplemented with 10× PBS (D5652-10X1L, Thermo Scientific, USA).

For a negative control, a mixture of 25% type-I collagen (10 mg ml^{-1}) and 75% sodium alginate

Table 1. Flow rates for cell-free extrusion (unit: ml min^{-1}).

	Inlet A	Inlet B	Inlet C	Inlet D
Double-layer device	1.5	3.0	—	—
Triple-layer device	0.7	1.5	3.0	—
Quadruple-layer device	0.2	0.7	1.5	3.0

(1.8% w/v) (denoted as C25–A75) was prepared. For the microstructural observations, 1 mm C25–A75 and neutralised type-I collagen (10 mg ml^{-1}) were pipetted into a 2 ml Eppendorf tube. Then, 500 μl of 100 mM $CaCl_2$ was added gently to the C25–A75 tube for alginate gelation. The tubes were incubated overnight at 37 °C for collagen gelation. Once completely gelated, the remaining $CaCl_2$ was eliminated, and the C25–A75 hydrogel was washed twice with PBS. Subsequently, both the C25–A75 and the collagen gel were dipped into liquid nitrogen for 3 min for rapid freezing. Then, they were chipped into small pieces before being lyophilised. The desiccated hydrogels were coated with metal by an Emitech K575X sputter coater (Quorum Technologies Ltd, UK). Microstructural images were acquired using an SU8220 Cold FE-SEM (Hitachi High-Tech Company, Japan) instrument. To observe cell growth, HASMCs were suspended in a 200 μl C25–A75 mixture and collagen (10 mg ml^{-1}) at a concentration of approximately 1.5×10^6 cells ml^{-1}. Then, the solutions were pipetted evenly into 20 mm-diameter gelatine-coated confocal dishes to form scaffolds with an approximate thickness of 600 μm. The dishes were incubated for 45 min at 37 °C to allow the collagen to gelate. The collagen hydrogel was supplied with fresh cell culture media and incubated at 37 °C under 5% CO_2; then, the C25–A75 scaffold was covered gently with 1 ml of 100 mM $CaCl_2$. Next, the $CaCl_2$ solution was removed. The C25–A75 hydrogel was supplied with fresh cell culture media and incubated at 37 °C under 5% CO_2. After 3 d, images were obtained using an IX53 inverted microscope (Olympus, Japan).

5.4. Cell culture

A cryopreserved HASMC (PCS-100-012, ATCC, USA) vial was thawed and incubated at 37 °C under 5% CO_2. During expansion, HASMCs were cultured in vascular cell basal media (PCS-100-030, ATCC, USA) supplemented with a vascular SMC growth kit (PCS-100-042, ATCC, USA). Before reaching 80% confluence, the cells were passaged using 0.05% trypsin ethylenediaminetetraacetic acid (EDTA) (25300062, Thermo Scientific, USA). The HASMCs were harvested after reaching approximately 80% confluence (after three to nine passages); then, they were suspended in type-I collagen at a density of approximately 6×10^6 cells ml^{-1}.

A vial of cryopreserved HUVECs (PCS-100-010, ATCC, USA) was thawed and incubated at 37 °C in a cell incubator containing 5% CO_2. During expansion, the HUVECs were cultured in vascular cell basal medium (PCS-100-030, ATCC, USA) supplemented with a Vascular endothelial growth factor (VEGF) endothelial cell growth kit (PCS-100-041, ATCC, USA). Before reaching approximately 80% confluence, the HUVECs were passaged using 0.05% trypsin EDTA. The HUVECs were harvested for the experiment when they reached approximately 80% confluence (within six to nine passages).

5.5. Coaxial laminar flow formation

To observe the effects of gravity on the coaxial laminar flow formation of hydrogels with double-, triple-, and quadruple-coaxial laminar flow devices, each device was assessed experimentally using the top-down and IG extrusion methods (figure 3). Table 1 describes the flow rates.

Figure 1 shows the configuration of the IG extruder. The coaxial laminar flow device was set under a $CaCl_2$ beaker; the base of the beaker was drilled using a diamond drill and connected with the outlet tube of the extruder. The gap between the outlet tube and the bottom hole was sealed with PDMS.

5.6. HASMC tubular collagen scaffold formation

A conceptual schematic of HASMC tubular collagen scaffold formation is presented in figure 1. Sodium alginate (1.5% w/v) was introduced via the bottom inlet as a core layer and the upper inlet as a shell layer. Type-I collagen containing HASMCs and $CaCl_2$ (150 mM) (2507-1400, DEAJUNG, Republic of Korea) was pumped into the middle inlet. The ion-crosslinking reactions between the sodium alginate layers and calcium ions (Ca^{2+}) in the collagen mixture and the $CaCl_2$ beaker (sterile and kept at 37 °C) caused a layer of collagen to become trapped and gelate between the sodium shell and core (figure 1).

The effects of the flow rate on the outer diameter of the core, the collagen layer, and the shell were investigated by varying the flow rates of the collagen and the sodium alginate core. The flow rate of the shell was fixed at 3 ml min^{-1}.

Following the extrusion, the scaffold was immersed in the beaker for 45 min to complete gelation. Then, the scaffold was gently collected, washed with PBS for 5 min to remove $CaCl_2$, supplied with fresh culture media for HASMCs, and incubated at 37 °C under 5% CO_2. After a 24 h incubation period, the alginate shell was removed using iris surgical scissors. During core maturation, the alginate core functioned as a mandrel to maintain the tubular shape

Table 2. Antibody list.

Primary antibodies	Dilution	Supplier	Cat. no.
α-Smooth muscle actin (mouse)	1:100	Thermo Scientific, USA	MA5-11547
CD31 (rabbit)	1:50	Thermo Scientific, USA	PA5-16301
Secondary antibodies	**Dilution**	**Supplier**	**Cat. no.**
Goat anti-mouse Alexa flour; 488 nm IgG	1:200	Thermo Scientific, USA	A32723
Goat anti-rabbit Alexa flour; 488 nm IgG	1:200	Abcam, USA	Ab150077
Goat anti-rabbit Alexa flour; 594 nm IgG	1:200	Abcam, USA	Ab150080

of the collagen layer. The mandrel was removed 16 d after its formation by using forceps. The scaffold with the core inside was put in a prewarm PBS petri dish (37 °C) then, a forceps was used to keep the scaffold, another forceps to grip the core and pull out of the scaffold. Alginate debris were flushed out by PBS pipetting. The culture media was replaced every 24 h.

5.7. Endothelialisation

The collagen scaffold was endothelialised after a maturation period of 16 d after formation. Because the C25–A75 scaffold had become too weak to handle at day 16, it was endothelialised after a 4 day maturation period. The endothelialisation setup was similar to that for the burst pressure test (figure 6(a)). One end of an HASMC scaffold (20 cm-long) was mounted via a one-way nonreturn valve to an infusing pump containing a prewarmed HUVEC suspension. The other end of the mounted scaffold was tightened with a rubber tie. The HUVEC suspension (3.5×10^6 cells ml^{-1}) was infused fully into the scaffold. The nonreturn valve ensured that the HUVEC suspension remained secure inside the scaffold. The scaffold was circumferentially rotated 180° every 10–20 min in a cell incubator, which ensured the development of a uniform HUVEC layer on the inner surface of the scaffold. After a 4 h rotation, the endothelialised scaffold was detached from the infusing pump.

To observe the formation of monolayer HUVECs on the inner surface of the scaffold, a 1 cm endothelialised scaffold segment was harvested and unfurled before immunostaining. The segment was fixed in 3.5% paraformaldehyde (PFA), permeabilised in 0.5% Triton X-100 for 5 min and blocked with 3% bovine serum albumin (BSA) for 1 h. Then, it was incubated in primary antibodies (table 2) for 24 h at 4 °C and in secondary antibodies (table 2) for 2 h at 37 °C. Nuclei were counterstained with DAPI at 37 °C for 10 min. Images were obtained using a FLUOVIEW FV1200 laser scanning confocal microscope (Olympus, Japan).

The immunostained images for the expression of platelet endothelial cell adhesion molecule protein (known as CD31) were used to quantify the confluency of the HUVECs. A 500 × 500 μm square frame was selected, and the intensity of the green light (CD31) was measured to determine the HUVEC confluency.

5.8. Histological analysis

The cell scaffolds were fixed overnight in 3.5% PFA (158127, Sigma−Aldrich, USA) before being dehydrated in ethanol. Before wax infiltration, xylene was used to displace the ethanol in the sample. Then, the samples were sliced into thicknesses of 10 μm using an RM2255 microtome (Leica Biosystems, Germany). Before staining, the paraffin wax in the sections was removed using xylene before rehydrating in ethanol and water. These processes were performed at the Bio-Medical Institute at Kyungpook National University Hospital, Dae-gu, Republic of Korea.

For Hematoxylin and eosin (H&E) staining, the slices were stained with Harris haematoxylin (3801561, Leica Biosystems, Germany) and alcoholic eosin Y515 (3801610, Leica Biosystems, Germany). Then, they were treated with ammonia buffer (50 ml deionised water + 0.15 ml ammonia solution [NH_4OH]). The H&E-stained slices were observed under a bright-field microscope (IX71, Olympus Corp., Tokyo, Japan).

For immunostaining, the slices were intermittently microwaved over 15 min in citrate buffer containing 10 mM sodium citrate (C8532, Sigma−Aldrich, USA) and 0.05% Tween 20 (P1379, Sigma−Aldrich, USA) at a pH of 6.0. Generally, the process of sample fixation can lead to protein cross-linking, which masks antigens and could inhibit binding between antigens and antibodies. The process of microwaving enables antibodies to access the target proteins within the samples. Then, the slices were blocked in 3% BSA and incubated in primary antibodies (table 2) for 24 h (4 °C). Sequentially, the slices were washed in PBS and incubated in secondary antibodies (table 2) for 2 h (37 °C). The nuclei were counterstained with DAPI for 10 min (37 °C). Finally, images were acquired using a BX53 digital upright microscope (Olympus, Japan).

The cell alignment within the scaffold wall was analysed using H&E slices. Regions of interest were selected from 10× magnified images using a square frame (100 × 100 μm). A circle-shaped cell was defined as a cell with a difference ratio between the maximum and minimum lengths of less than 25% of the minimum length. This meant that elongated cells were cells whose difference ratio between the maximum and minimum lengths of the nucleus was higher than 25% of the minimum length. The cell

alignment was measured according to the angle made by the maximum length and the horizontal line of the image. The similarity in cell alignment was revealed using the SD of the cell angles. The length and angle measurements were obtained using ImageJ software (version 1.51 h, Fiji, NIH Image, USA). The wall thickness of the cell scaffolds was taken as the average of the thickest and thinnest regions.

5.9. Mechanical analysis

The burst pressure of the cell scaffold was measured using a lab-made tool (figure 6(a)) comprising a pulsatile pump (70-4504, Harvard Apparatus, USA), a 3 mm plastic one-way nonreturn valve, a pressure gauge (169-05, 0–760 mmHg, GAST, USA), and a glass connector. The cell scaffold (4 cm-long) was mounted to the glass connector and tightened at the end using rubber ties (figure 6). Deionised water was pumped repeatedly at a flow rate of 10 ml min^{-1} for 10 s followed by 5 s of rest. The burst pressure was recorded until the scaffold burst. Scaffolds with three different collagen concentrations (6 mg ml^{-1} [6-col], 8 mg ml^{-1} [8-col], and 10 mg ml^{-1} [10-col]) were selected to measure the burst pressure compared with C25–A75 scaffolds.

To measure the longitudinal breaking force, one end of the scaffold was fixed, and the other end was stretched until tearing occurred (figure 6(d)). One end of a 4 cm-long scaffold was tightened at the bottom of a glass beaker containing 1× PBS. The other end was attached to a glass connector linked to a digital force gauge (FG-104-1K, Handking, Republic of Korea). The upright scaffold was stretched at 0.5 mm s^{-1} until tearing occurred.

To measure the circumferential breaking force, a 1 cm-long scaffold was loaded onto a pair of glass pegs (figure 6(g)). One peg was fixed to the bottom of a glass beaker containing 1× PBS, while the other was connected to the digital force gauge. The stretching rate was 0.5 mm s^{-1} .

5.10. Suture retention strength measurement

A lab-made system was used to measure the suture retention strength of the maturated vessels (figure 8(a)). One end of a 3 cm-long vessel was tightened to the PDMS pair. A thread was pushed through the vessel's wall using a supplied needle. The attached thread was pulled at 1 mm s^{-1} until the vessel broke.

5.11. Animals

All animal experiments were conducted in accordance with the principles and standards of laboratory animal welfare and ethics under official approval issued by the Institutional Animal Care and Use Committee (GIG-22-030 and GIG-22-040) of the University of Ulsan. A total of 12 C57BL/6 mice (3–8 weeks old, 15–35 g) were purchased from KOATECH (Pyeongtaek, Republic of Korea). The mice were housed in a facility with 60% humidity at 24 °C with a 12 h light/dark cycle and with free access to food and water.

5.12. Adhesion and haemolysis test

Fresh blood was collected from 5 week-old mice and then heparinised. The harvested blood was gently injected into the vessel lumen (0.1 ml min^{-1}) with or without the endothelial layer for 30 min at 37 °C. The vessel was slowly flushed with PBS afterwards to remove unattached RBCs and platelets, fixed with 2.5% glutaraldehyde and lyophilised for scanning electron microscopy. The desiccated hydrogels were metal coated with an Emitech K575X sputter coater (Quorum Technologies Ltd, United Kingdom). Microstructural images were acquired using an SU8220 Cold FE-SEM (Hitachi High Technologies Co., Ltd, Japan). Attached RBCs and platelets were counted in areas of 100 μm^2 from each specimen.

For the haemolysis test, RBCs were obtained from the heparinised blood by centrifugation at 600 × g for 10 min and washed with PBS. The RBC pellet from 1 ml of fresh blood was suspended and diluted at a 1:10 ratio with PBS for assays. Suspensions of RBCs in PBS and deionised water were considered negative and positive controls, respectively. The vessels matured for 4 d after endothelialisation were incubated for 1 h and 3 h respectively at 37 °C in 1 ml of diluted RBC suspension. After that, the vessels were removed. The RBC suspensions were centrifuged at 600 × *g* for 10 min. The light absorbance of the supernatant was measured at 415 nm to determine the percentage of haemolysis cells, which was calculated using equation (3).

$$\text{Haemolysis}\,(\%) = \frac{\text{Sample absorbance} - \text{Negative control absorbance}}{\text{Positive control absorbance} - \text{Negative control absorbance}} \times 100. \quad (3)$$

5.13. Subcutaneous implantation

Considering the mouse size, a 1 mm diameter vessel was extruded using the proposed IG method and another triple-layer device with smaller-diameter glass capillaries (0.58 mm inner diameter for the inlets, 1.5 mm for the middle pipe, 1.8 mm for the outlet) (figure S14). The glass capillaries were tapered to reach 0.4 mm for the inlet A, 1.2 for the middle pipe figure S14(a). The flow rates for the inlet A, inlet B, inlet C were 0.35 ml min^{-1}, 0.8 ml min^{-1},

and 0.52 ml min^{-1}, respectively. Once matured, the outer diameter of the vessel here was about 1 mm and the inner diameter was measured at approximately 0.82 mm (video S6).

A mouse (∼5 weeks of age, ∼25 g) was anaesthetised by an intraperitoneal injection of tribromoethanol (∼240 mg kg^{-1}). The mouse was completely anaesthetised in 5 min. Nair gel and povidone-iodine 10% were used to remove hair and disinfect the dorsal skin of the mouse before surgery. The dorsal skin was opened using sterilised scissors and fine forceps. The size of the opened skin was ∼15 mm long and ∼10 mm wide. A fabricated vessel (∼1 mm-diameter, ∼10 mm long) was placed in the opened site. The dorsal skin was sutured using black silk suture 4-0. Postoperatively, the mouse was injected with buprenorphine (1 mg kg^{-1}) painkiller and allowed to recover on a heating pad for 2 h. After that, the mouse was placed in a single cage with access to food and water. The mouse was anaesthetised one more time to harvest the implanted vessel on day 14. The implanted vessel was dissected, fixed with 3.5% PFA overnight, and then histologically processed.

5.14. Statistical analysis

The results are presented as the means ± SDs. Comparisons between two groups were performed using a two-tailed Student's t test in Prism 6.01 (GraphPad, USA), and a value of $p < 0.05$ was considered statistically significant. Finally, the sample sizes are noted in the figure captions.

Data availability statement

The data that support the findings of this study are available upon reasonable request from the authors.

Acknowledgments

This work was supported by Korean Medical Device Development Fund (KMDF PR 20210527 0006-2021-01), Republic of Korea.

Conflict of interest

The authors declare no competing financial or non-financial interests.

Author contributions

V T D was involved in the design of the experiments, conducted the experiments and analysed the data, and wrote the paper. C T N, H L P, V P L, T T D, and C C conducted the experiments and analysed the data. J S, C C, S H B trained techniques for others and provided facilities for the experiments and discussed the results, commented on the paper. K K was the principal investigator, initiated the project, wrote the paper, and approved the final version.

ORCID iDs

Van Thuy Duong https://orcid.org/0000-0002-7131-4272
Chanh Trung Nguyen https://orcid.org/0000-0002-3517-9499
Huu Lam Phan https://orcid.org/0000-0002-2025-5946
Van Phu Le https://orcid.org/0000-0001-8104-4133
Thao Thi Dang https://orcid.org/0000-0001-7175-1934
Cholong Choi https://orcid.org/0000-0001-9722-8842
Jongmo Seo https://orcid.org/0000-0002-1889-7405
Chaenyung Cha https://orcid.org/0000-0002-3615-0145
Sung Hoon Back https://orcid.org/0000-0001-8029-1298
Kyo-in Koo https://orcid.org/0000-0003-4173-9218

References

[1] Adamski M G and Baird A E 2013 Genetics of stroke *Emery and Rimoin's Principles and Practice of Medical Genetics* 6th, ed D Rimoin, R Pyeritz and B Korf (Academic) ch 123, pp 1–20
[2] Allison M A, Ho E, Denenberg J O, Langer R D, Newman A B, Fabsitz R R and Criqui M H 2007 Ethnic-specific prevalence of peripheral arterial disease in the United States *Am. J. Prev. Med.* **32** 328–33
[3] Libby P, Buring J E, Badimon L, Hansson G K, Deanfield J, Bittencourt M S, Tokgözoğlu L and Lewis E F 2019 Atherosclerosis *Nat. Rev. Dis. Primers* **5** 56
[4] Campia U, Gerhard-Herman M, Piazza G and Goldhaber S Z 2019 Peripheral artery disease: past, present, and future *Am. J. Med.* **132** 1133–41
[5] Hamburg N M and Balady G J 2011 Exercise rehabilitation in peripheral artery disease *Circulation* **123** 87–97
[6] Fowkes F G R, Aboyans V, Fowkes F J I, McDermott M M, Sampson U K A and Criqui M H 2017 Peripheral artery disease: epidemiology and global perspectives *Nat. Rev. Cardiol.* **14** 156–70
[7] Tsai T T *et al* 2015 The contemporary safety and effectiveness of lower extremity bypass surgery and peripheral endovascular interventions in the treatment of symptomatic peripheral arterial disease *Circulation* **132** 1999–2011
[8] Hiramoto J S, Teraa M, de Borst G J and Conte M S 2018 Interventions for lower extremity peripheral artery disease *Nat. Rev. Cardiol.* **15** 332–50
[9] Organ Procurement and Transplantation Network Organ Donation Statistics (available at: www.organdonor.gov/statistics-stories/statistics.html) (Accessed 18 April 2021)
[10] Hacken B A, Keyt L K, Leland D P, LaPrade M D, Camp C L, Levy B A, Stuart M J and Krych A J 2020 A novel scoring instrument to assess donor site morbidity after anterior cruciate ligament reconstruction with a patellar tendon autograft at 2-year follow-up using contemporary graft-harvesting techniques *Orthop. J. Sports Med.* **8** 2325967120925482
[11] Xue L and Greisler H P 2003 Biomaterials in the development and future of vascular grafts *J. Vasc. Surg.* **37** 472–80

[12] Elliott M B et al 2019 Regenerative and durable small-diameter graft as an arterial conduit *Proc. Natl Acad. Sci.* **116** 12710
[13] Skorpil J and Hajek T 2012 Coronary artery bypass grafting (CABG) *Minimized Cardiopulmonary Bypass Techniques and Technologies* ed T Gourlay and S Gunaydin (Woodhead Publishing) ch 11, pp 176–88
[14] MedicalExpo Synthetic vascular prostheses (available at: www.medicalexpo.com/) (Accessed 18 April 2021)
[15] Mahara A, Li M, Ohya Y and Yamaoka T 2020 Small-diameter synthetic vascular graft immobilized with the REDV peptide reduces early-stage fibrin clot deposition and results in graft patency in rats *Biomacromolecules* **21** 3092–101
[16] Matsuzaki Y, John K, Shoji T and Shinoka T 2019 The evolution of tissue engineered vascular graft technologies: from preclinical trials to advancing patient care *Appl. Sci.* **9** 1274
[17] Fiqrianti I A, Widiyanti P, Manaf M A, Savira C Y, Cahyani N R and Bella F R 2018 Poly-L-lactic acid (PLLA)-chitosan-collagen electrospun tube for vascular graft application *J. Funct. Biomater.* **9** 32
[18] Park S, Kim J, Lee M-K, Park C, Jung H-D, Kim H-E and Jang T-S 2019 Fabrication of strong, bioactive vascular grafts with PCL/collagen and PCL/silica bilayers for small-diameter vascular applications *Mater. Des.* **181** 108079
[19] Carrabba M and Madeddu P 2018 Current strategies for the manufacture of small size tissue engineering vascular grafts *Front. Bioeng. Biotechnol.* **6** 41
[20] Skovrind I, Harvald E B, Juul Belling H, Jørgensen C D, Lindholt J S and Andersen D C 2019 Concise review: patency of small-diameter tissue-engineered vascular grafts: a meta-analysis of preclinical trials *Stem Cells Transl. Med.* **8** 671–80
[21] Kannan R Y, Salacinski H J, Butler P E, Hamilton G and Seifalian A M 2005 Current status of prosthetic bypass grafts: a review *J. Biomed. Mater. Res.* B **74B** 570–81
[22] Goodman W G et al 2000 Coronary-artery calcification in young adults with end-stage renal disease who are undergoing dialysis *New Engl. J. Med.* **342** 1478–83
[23] Chong D S T, Constantinou J, Davis M and Hamilton G 2016 Calcification of a synthetic renovascular graft in a child *EJVES Short Rep.* **33** 13–15
[24] L'Heureux N, Pâquet S, Labbé R, Germain L and Auger F 1998 A completely biological tissue-engineered human blood vessel *FASEB J.* **12** 47–56
[25] L'Heureux N et al 2006 Human tissue-engineered blood vessels for adult arterial revascularization *Nat. Med.* **12** 361–5
[26] Costa M, Cerqueira M T, Santos T C, Sampaio-Marques B, Ludovico P, Marques A P, Pirraco R P and Reis R L 2017 Cell sheet engineering using the stromal vascular fraction of adipose tissue as a vascularization strategy *Acta Biomater.* **55** 131–43
[27] Meghezi S, Seifu D G, Bono N, Unsworth L, Mequanint K and Mantovani D 2015 Engineering 3D cellularized collagen gels for vascular tissue regeneration *J. Vis. Exp.* **100** e52812
[28] Nasr A Y 2012 The radial artery and its variations: anatomical study and clinical implications *Folia Morphol.* **71** 252–62 (in English)
[29] Kandinata N and Van Fossen K *Anatomy, Abdomen and Pelvis, Epigastric Artery* (available at: www.ncbi.nlm.nih.gov/books/NBK537156/) (Accessed 2021)
[30] Yang G and Chung K C 2018 Procedure 78—free anterolateral thigh flap *Operative Techniques: Hand and Wrist Surgery* 3rd edn, ed K C Chung (Elsevier) pp 713–9
[31] Beniwal S, Bhargava K and Kausik S K 2014 Size of distal radial and distal ulnar arteries in adults of southern Rajasthan and their implications for percutaneous coronary interventions *Indian Heart J.* **66** 506–9
[32] Mahdi Fathi E H, Fathi H R and Abbasi A 2008 The anatomy of superficial inferior epigastric artery flap *Acta Cir. Bras.* **23** 429–34
[33] Lubek J E and Engroff S L 2012 Anterolateral thigh flap *Current Therapy in Oral and Maxillofacial Surgery* ed S C Bagheri, R B Bell and H A Khan (W.B. Saunders) ch 71, pp 584–8
[34] Gold K A, Saha B, Rajeeva Pandian N K, Walther B K, Palma J A, Jo J, Cooke J P, Jain A and Gaharwar A K 2021 3D bioprinted multicellular vascular models *Adv. Healthcare Mater.* **10** 2101141
[35] Tabriz A G, Hermida M A, Leslie N R and Shu W 2015 Three-dimensional bioprinting of complex cell laden alginate hydrogel structures *Biofabrication* **7** 045012
[36] Norotte C, Marga F S, Niklason L E and Forgacs G 2009 Scaffold-free vascular tissue engineering using bioprinting *Biomaterials* **30** 5910–7
[37] Gao Q et al 2017 3D bioprinting of vessel-like structures with multilevel fluidic channels *ACS Biomater. Sci. Eng.* **3** 399–408
[38] Shin S-J, Park J-Y, Lee J-Y, Park H, Park Y-D, Lee K-B, Whang C-M and Lee S-H 2007 'On the Fly' continuous generation of alginate fibers using a microfluidic device *Langmuir* **23** 9104–8
[39] Onoe H et al 2013 Metre-long cell-laden microfibres exhibit tissue morphologies and functions *Nat. Mater.* **12** 584
[40] Koo K-I, Lenshof A, Huong L T and Laurell T 2021 Acoustic cell patterning in hydrogel for three-dimensional cell network formation *Micromachines* **12** 3
[41] Duong V-T, Kim J P, Kim K, Ko H, Hwang C H and Koo K-I 2018 Three-dimensional bio-printing technique: trend and potential for high volume implantable tissue generation (in Ko) *J. Biomed. Eng. Res.* **39** 188–207
[42] Van Thuy Duong Y L, Nguyen T, Choi M, Lam Phan H, Lee Y, Park H, Shin D and Koo K-I 2017 Twenty-day culturing of tubular scaffolds using micro-connector with heart-mimicking medium pumping for blood vessel modeling *The 21st International Conference on Miniaturized Systems for Chemistry and Life Sciences (MicroTAS 2017)*
[43] Oh S, Duong V T, Phan H L, Hwang C H and Koo K-I 2019 Enhance cell confluence using gradually-degraded alginate-collagen material for tunica intermedia formation *23rd Int. Conf. on Miniaturized Systems for Chemistry and Life Sciences, MicroTAS 2019* (Congress Center Basel Basel) pp 520–1
[44] Duong V T, Oh S, Phan H L, Hwang C H and Koo K-I 2019 Over-five-millimeter diameter alginate-collagen endothelialized tubular scaffold formation *23rd Int. Conf. on Miniaturized Systems for Chemistry and Life Sciences, MicroTAS 2019* (Congress Center Basel Basel) pp 524–5
[45] Duong V T, Oh S, Nguyen C T, Hwang C H and Koo K-I 2018 Multi-lumen tubular calcium-alginate cell-laden scaffold formation for 3D bioprinting *22nd Int. Conf. on Miniaturized Systems for Chemistry and Life Sciences, MicroTAS 2018* (*Kaohsiung, Taiwan*) pp 2286–7
[46] Nguyen C T, Duong V T, Hwang C H and Koo K I 2022 Angiogenesis in free-standing two-vasculature-embedded scaffold extruded by two-core laminar flow device *Int. J. Bioprinting* **8** 557
[47] Nguyen T T T, Duong V T, Huong L T and Koo K I 2022 3D printing for human tendon-muscle gradient scaffolds engineering *2022 Int. Workshop on Intelligent Systems (IWIS)* (*17–19 August 2022*) pp 1–3
[48] Duong V T et al 2017 Twenty-day culturing of tubular scaffolds using micro-connector with heart-mimicking medium pumping for blood vessel modeling *MicroTAS 2017* (*Savannah, Georgia 31402 USA, 22–26 October 2017*)
[49] Edri R et al 2019 Personalized hydrogels for engineering diverse fully autologous tissue implants *Adv. Mater.* **31** 1803895
[50] Gao G, Park J Y, Kim B S, Jang J and Cho D-W 2018 Coaxial cell printing of freestanding, perfusable, and functional in vitro vascular models for recapitulation of native vascular

endothelium pathophysiology *Adv. Healthcare Mater.* **7** 1801102
[51] Duong V T *et al* 2018 Cell attachment on inside-outside surface and cell encapsulation in wall of microscopic tubular scaffolds for vascular tissue-like formation *2018 40th Annual International Conference of the IEEE Engineering in Medicine and Biology Society (EMBC) (18–21 July 2018)* pp 4198–201
[52] Oh D, Lee S, Koo K-I and Seo J-M 2015 Microscopic tubular cell organization for artificial vascularization *6th European Conf. Int. Federation for Medical and Biological Engineering* (Springer International Publishing) pp 322–5
[53] Duong V T, Dang -T-T, Kim J P, Kim K, Ko H, Hwang C H and Koo K-I 2019 Twelve-day medium pumping into tubular cell-laden scaffold using a lab-made PDMS connector *Eur. Cells Mater.* **38** 1–13
[54] Duong V T, Dang T T, Hwang C H, Back S H and Koo K-I 2020 Coaxial printing of double-layered and free-standing blood vessel analogues without ultraviolet illumination for high-volume vascularised tissue *Biofabrication* **12** 045033
[55] Pi Q *et al* 2018 Digitally tunable microfluidic bioprinting of multilayered cannular tissues *Adv. Mater.* **30** 1706913
[56] Gao G *et al* 2017 Tissue engineered bio-blood-vessels constructed using a tissue-specific bioink and 3D coaxial cell printing technique: a novel therapy for ischemic disease *Adv. Funct. Mater.* **27** 1700798
[57] Gao G *et al* 2019 Tissue-engineering of vascular grafts containing endothelium and smooth-muscle using triple-coaxial cell printing *Appl. Phys. Rev.* **6** 041402
[58] Liang Q, Gao F, Zeng Z, Yang J, Wu M, Gao C, Cheng D, Pan H, Liu W and Ruan C 2020 Coaxial scale-up printing of diameter-tunable biohybrid hydrogel microtubes with high strength, perfusability, and endothelialization *Adv. Funct. Mater.* **30** 2001485
[59] Pepelanova I, Kruppa K, Scheper T and Lavrentieva A 2018 Gelatin-methacryloyl (GelMA) hydrogels with defined degree of functionalization as a versatile toolkit for 3D cell culture and extrusion bioprinting *Bioengineering* **5** 55
[60] Wang M *et al* 2022 Molecularly cleavable bioinks facilitate high-performance digital light processing-based bioprinting of functional volumetric soft tissues *Nat. Commun.* **13** 3317
[61] Rehm B, Consultant D, Haghshenas A, Paknejad A S and Schubert J 2008 Situational problems in MPD *Managed Pressure Drilling* ed B Rehm, J Schubert, A Haghshenas, A S Paknejad and J Hughes (Gulf Publishing Company) ch 2, pp 39–80
[62] Kundu P K, Cohen I M and Dowling D R 2016 Laminar flow *Fluid Mechanics* 6th edn, ed P K Kundu, I M Cohen and D R Dowling (Academic) ch 9, pp 409–67
[63] Henriksen K and Karsdal M A 2016 Type I collagen *Biochemistry of Collagens, Laminins and Elastin* ed M A Karsdal (Academic) ch 1, pp 1–11
[64] Henriksen K and Karsdal M A 2019 Type I collagen *Biochemistry of Collagens, Laminins and Elastin* 2nd edn, ed M A Karsdal (Academic) ch 1, pp 1–12
[65] Kefallinou D, Grigoriou M, Boumpas D T, Gogolides E and Tserepi A 2020 Fabrication of a 3D microfluidic cell culture device for bone marrow-on-a-chip *Micro Nano Eng.* **9** 100075
[66] Costa P F, Albers H J, Linssen J E A, Middelkamp H H T, van der Hout L, Passier R, van den Berg A, Malda J and van der Meer A D 2017 Mimicking arterial thrombosis in a 3D-printed microfluidic *in vitro* vascular model based on computed tomography angiography data *Lab Chip* **17** 2785–92
[67] Allen P, Melero-Martin J and Bischoff J 2011 Type I collagen, fibrin and PuraMatrix matrices provide permissive environments for human endothelial and mesenchymal progenitor cells to form neovascular networks *J. Tissue Eng. Regen. Med.* **5** e74–e86
[68] Advanced BioMatrix Collagen concentration vs gel stiffness (available at: https://advancedbiomatrix.com/collagenconcentrationvideo.html) (Accessed 2021)
[69] Narita T, Yunoki S, Ohyabu Y, Yahagi N and Uraoka T 2016 In situ gelation properties of a collagen-genipin sol with a potential for the treatment of gastrointestinal ulcers *Med. Devices* **9** 429–39
[70] Ashton R S, Banerjee A, Punyani S, Schaffer D V and Kane R S 2007 Scaffolds based on degradable alginate hydrogels and poly(lactide-co-glycolide) microspheres for stem cell culture *Biomaterials* **28** 5518–25
[71] Lee K Y and Mooney D J 2012 Alginate: properties and biomedical applications *Prog. Polym. Sci.* **37** 106–26
[72] Hoenicka M, Schrammel S, Bursa J, Huber G, Bronger H, Schmid C and Birnbaum D E 2013 Development of endothelium-denuded human umbilical veins as living scaffolds for tissue-engineered small-calibre vascular grafts *J. Tissue Eng. Regen. Med.* **7** 324–36
[73] Latimer C A, Nelson M, Moore C M and Martin K E 2014 Effect of collagen and elastin content on the burst pressure of human blood vessel seals formed with a bipolar tissue sealing system *J. Surg. Res.* **186** 73–80
[74] Anthony B B and Taylor M *Histology, Blood Vascular System* (StatPearls) (available at: www.ncbi.nlm.nih.gov/books/NBK553217/) (Accessed 15 Feburay 2021)
[75] Adel K A, Ronald A B and Paul M H Anatomy atlases: section 8: cardiovascular system (available at: www.anatomyatlases.org/MicroscopicAnatomy/Section08/Section08.shtml) (Accessed 17 October 2019)
[76] Park J and Tallquist M D 2018 Cardiac fibroblast *Encyclopedia of Cardiovascular Research and Medicine* ed R S Vasan and D B Sawyer (Elsevier) pp 420–33
[77] Williams I R 1998 Fibroblasts *Encyclopedia of Immunology* 2nd edn, ed P J Delves (Elsevier) pp 905–9
[78] Montesano R, Vassalli J D, Baird A, Guillemin R and Orci L 1986 Basic fibroblast growth factor induces angiogenesis *in vitro Proc. Natl Acad. Sci.* **83** 7297
[79] Nguyen D-H T, Stapleton S C, Yang M T, Cha S S, Choi C K, Galie P A and Chen C S 2013 Biomimetic model to reconstitute angiogenic sprouting morphogenesis *in vitro Proc. Natl Acad. Sci.* **110** 6712
[80] Silvagno F, Follenzi A, Arese M, Prat M, Giraudo E, Gaudino G, Camussi G, Comoglio P M and Bussolino F 1995 *In vivo* activation of met tyrosine kinase by heterodimeric hepatocyte growth factor molecule promotes angiogenesis *Arterioscler. Thromb. Vasc. Biol.* **15** 1857–65
[81] Yang Z, Arnet U, Bauer E, von Segesser L, Siebenmann R, Turina M and Lüscher T F 1994 Thrombin-induced endothelium-dependent inhibition and direct activation of platelet-vessel wall interaction. Role of prostacyclin, nitric oxide, and thromboxane A2 *Circulation* **89** 2266–72
[82] Zilla P *et al* 1994 Clinical *in vitro* endothelialization of femoropopliteal bypass grafts: an actuarial follow-up over three years *J. Vasc. Surg.* **19** 540–8
[83] Magometschnigg H, Kadletz M, Vodrazka M, Dock W, Grimm M, Grabenwöger M, Minar E, Staudacher M, Fenzl G and Wolner E 1992 Prospective clinical study with *in vitro* endothelial cell lining of expanded polytetrafluoroethylene grafts in crural repeat reconstruction *J. Vasc. Surg.* **15** 527–35
[84] Choi W S, Joung Y K, Lee Y, Bae J W, Park H K, Park Y H, Park J-C and Park K D 2016 Enhanced patency and endothelialization of small-caliber vascular grafts fabricated by coimmobilization of heparin and cell-adhesive peptides *ACS Appl. Mater. Interfaces* **8** 4336–46

[85] Li X, Xu J, Nicolescu C T, Marinelli J T and Tien J 2016 Generation, endothelialization, and microsurgical suture anastomosis of strong 1-mm-diameter collagen tubes *Tissue Eng.* A **23** 335–44
[86] Pensalfini M, Meneghello S, Lintas V, Bircher K, Ehret A E and Mazza E 2018 The suture retention test, revisited and revised *J. Mech. Behav. Biomed. Mater.* **77** 711–7
[87] Meng X, Wang X, Jiang Y, Zhang B, Li K and Li Q 2019 Suture retention strength of P(LLA-CL) tissue-engineered vascular grafts *RSC Adv.* **9** 21258–64
[88] Fujita H and Kato T 1964 On the Navier-Stokes initial value problem. I *Arch. Ration. Mech. Anal.* **16** 269–315
[89] AIM Biotech Collagen gel preparation protocol (available at: www.youtube.com/watch?v=x3Rmj3ALoOI) (Accessed 1 January 2019)